Title

Isotope- and Thickness-Dependent Friction of Water Layers Intercalated Between Graphene and Mica

Permalink

https://escholarship.org/uc/item/05q8m4j0

Journal

Tribology Letters, 66(1)

ISSN

1023-8883

Authors

Lee, Hyunsoo
Ko, Jae-Hyeon
Song, Hee Chan
et al.

Publication Date

2018-03-01

DOI

10.1007/s11249-018-0984-3

Peer reviewed

Isotope and Thickness-Dependent Friction of Water Layers Intercalated between Graphene and Mica

Hyunsoo Lee[1] · Jae-Hyeon Ko[2] · Hee Chan Song[1,3] · Miquel Salmeron[4] · Yong-Hyun Kim[2] · Jeong Young Park[1,3]

Abstract The lubricating properties of water have been discussed extensively for millennia. Water films can exhibit high friction in the form of cold ice, or act as lubricants in skating and skiing when liquid. At the fundamental level, friction is the result of a balance between the rate of energy generation by phonon excitation during sliding, and drainage of the energy from the interface by coupling with bulk atoms. Using atomic force microscopy (AFM) we found that when H_2O water intercalates between graphene and mica it increases the friction between the tip and the substrate, dependent on the thickness of water and graphene layers, while the magnitude of friction increase was reduced by D_2O water intercalation. With the help of first-principles density-functional theory calculations we explain this unexpected behavior by the increased spectral range of vibration modes of graphene caused by water, and by the better overlap of the graphene vibration modes with the mica phonons, which favors more efficient dissipation of the energy. The larger increase in friction with H_2O vs D_2O shows that the high-frequency vibration modes of water molecules play a very important role in the transfer of the vibrational energy of the graphene to the phonon bath of the substrate.

E-mail: Yong-Hyun Kim (yong.hyun.kim@kaist.ac.kr)
Jeong Young Park (jeongypark@kaist.ac.kr)

[1]Center for Nanomaterials and Chemical Reactions, Institute for Basic Science (IBS), Daejeon 34141, South Korea.
[2]Graduate School of Nanoscience and Technology, Korea Advanced Institute of Science and Technology (KAIST), Daejeon 34141, South Korea.
[3]Graduate School of EEWS, Korea Advanced Institute of Science and Technology (KAIST), Daejeon 34141, South Korea.
[4]Materials Science Division, Lawrence Berkeley National Laboratory, Berkeley, California 94720, USA.

Keywords Phonon mode · Excitation and transfer · Water molecules · Nanoscale friction

1. Introduction

Friction phenomena are at the heart of the mechanical engineering field of tribology. Fundamental studies of friction are difficult because the interface is difficult to access using conventional microscopy and spectroscopy methods. In addition, multiple energy dissipation phenomena (e.g., electronic excitation, atomic vibration, chemical reactions, and other energy dissipation processes) act simultaneously and ultimately transfer the energy to bulk phonon modes[1-5].

When two bodies in contact slide past each other friction causes dissipation of mechanical energy, normally converted to heat. At the fundamental level the first step is the excitation of vibrations of the surface atoms. The energy of these vibrations is then transferred to the phonon modes of the substrate[2]. These two processes, excitation and transfer, can be influenced by interposed films (the lubricants) that alter their effectiveness. Therefore, to gain a fundamental understanding of such complex phenomena, it is important to study simplified systems where the contacting surfaces and interposed lubricant can be characterized as precisely as possible.

The role of water in frictional energy dissipation has been debated for decades. While films of cold ice exhibit high friction, a layer of liquid water under skis acts as a lubricant[6, 7]. To resolve these long-standing issues in tribology, we chose a system consisting of graphene deposited on mica. Graphene, which is composed of sp^2-bonded carbon atoms in a honeycomb lattice[8, 9], is an excellent model system for studies of intercalated water, as shown recently using atomic force microscopy (AFM) [10-12]. The first adsorbed ice-like water adlayer at the interface between graphene and mica is stably observed using AFM at room temperature under ambient conditions[10]. This first ice-like water layer grows with its crystallographic directions aligned with those of the mica substrate[13]. The second layer grows by molecular diffusion along the zigzag directions of the carbon–carbon bonds in the graphene[14]. The Stranski–Krastanov growth mode of water layer between graphene and mica is suggested by AFM experiments and molecular dynamics (MD) simulation[15]. In addition, Severin *et al.* investigated the phase separation of adsorbed ethanol and water at the interface of graphene/mica using scanning force microscopy (SPM) [16]. Cheng *et al.* demonstrated that the adsorbed ice-like water layer on mica can play role of a lubricant layer for 3-dimensional water nanodroplets between graphene and mica[17].

The nanoscale frictional behavior of the mechanical exfoliated graphene on silica was described by the puckering effect which is originated from the susceptibility of atomically thin layer to out-of-plane elastic deformation[18]. This puckering effect leads the graphene layer thickness dependence of friction while the strong adhesive force between graphene and mica prevents the friction change. The anisotropy of friction on the mechanical exfoliated monolayer graphene on silica substrates was also clearly observed using AFM[2, 19]. The electron-phonon coupling affects the friction difference between mono- and bilayer graphene on silicon carbide substrate[20]. The nanoscale friction of graphene is also easily influenced by the flexibility that was confirmed by the chemical modification of graphene surface such as fluorination[21, 22] and hydrogenation[23, 24]. Furthermore, the higher effective shear strength on hydrogenated than deuterated silicon and diamond surface was revealed under ultrahigh vacuum[3].

In this paper, we investigated the effects of adsorbed water molecules between graphene and hydrophilic mica on friction of graphene after exposure to moist air using friction force microscopy (FFM) at ambient conditions. The friction of monolayer graphene on the first ice-like normal and deuterated water adlayer is the ~3 and ~1.5 times larger than on the directly contacted graphene on mica, respectively. Furthermore, we show that the increase of the number of water layer leads the enhancement on friction of graphene due to the additional phonon channels by water layer, while the friction decreases with the increase of the number of graphene covered layer on water layer. The contribution of water vibration modes to energy transfer from the graphene to the mica substrate was ascertained by isotopic substitution experiments where H_2O is replaced by D_2O, as described below.

2. Experimental Methods

The mechanical exfoliation method[25] was used to form the mono-, bi-, and multi-layer graphene on SiO_2/Si (300 nm for silica thickness) and freshly cleaved muscovite mica surface (Grade V5, Ted Pella, Inc) using adhesive tape and kish graphite

(Grade 300, Graphene Supermarket) in air (45 ~ 50 % for relative humidity (RH), 22 ~ 24 ℃ for room temperature). The digitales thermo-hygrometer (klima guard, TFA-GERMANY) with covering RH of 1 % ~ 99 % ± 3 % was used for monitoring RH and temperature changes. The water layer between graphene and mica is formed in the cylindrical glass cell (140 mm for diameter, 150 mm for height) with a beaker of deionized water (or deuterium oxide, 99.9 atom% D, Aldrich). The RH increases over 95 % within a few hours in the cylindrical glass cell at room temperature (~23 ℃). The vacuum annealing of water intercalated graphene on mica sample was performed at 400 ℃ for 2h under 3.5×10^{-3} Torr.

Kelvin probe force microscopy (KPFM) and FFM measurements were carried out at ambient conditions (46–50% for RH and 23–24 ℃ for temperature) using an environmental AFM (AFM 5500, Agilent). A Pt/Ir-coated EFM tip (PPP-EFM-50, Nanosensor) with the typical resonance frequency of 75 kHz and spring constant of 2.8 N/m is used for KPFM measurements of water intercalated graphene on mica. Using double lock-in techniques, CPD were simultaneously obtained with topographical image by using two frequencies (ω_{mech} = 75 kHz, ω_{elec} = 10 kHz) via interleave (lift) mode with amplitude modulation. Here, ω_{mech} is the frequency for topographic information through the mechanical vibration of cantilever and ω_{elec} is the other frequency for the surface potential through the electric modulation. The tip bias V_{dc} was applied to getting the electrostatic interaction between tip and sample. A SiO_2/Si AFM tip (PPP-LFMR-50) with the typical spring constant of 0.2 N/m is used for FFM measurements on the water intercalated graphene on mica. Since the time-dependent behavior of the frictional force was not shown during the measurements, FFM experiment was performed in the elastic regime. A TGF11 silicon calibration grating sample (MikroMasch) was used for the friction calibration[26, 27]. The AFM experiments at low humidity (8%) were performed by purging N_2 gas inside the environmental glass cell. Raman spectra were measured at ambient conditions with a ARAMS micro Raman spectroscope (Horiba Jobin Yvon, France) using 1800 lines/mm grating, 10 s acquisition time, 0.5 mW power, and 514.5 nm laser excitation.

First-principles density-functional theory (DFT) calculations were performed to obtain phonon density of states (DOS) of H_2O and D_2O intercalated graphene on mica.

We employed *ab initio* plane-wave methods with the Perdew−Burke−Ernzerhof exchange−correlation functional [41], as implemented in the Vienna *ab initio* simulation package (VASP) [42, 43]. A kinetic energy cutoff of 500 eV and all-electron-like projector-augmented wave potentials were used [44]. Atomic forces are fully relaxed until the maximum Hellmann-Feynman force was less than 0.001 eV/Å. To describe the van der Waals interactions, we used the Grimme dispersion-corrected DFT-D2 method [45]. To simplify the phonon DOS calculations, we used a (2 × 2) graphene unit cell with a fixed grephene lattice constant. The lattice mismatch between graphene and water layer (or mica) is ~12 % (or ~5 %). For phonon calculations, we used the finite displacement method and phonopy program [46, 47].

3. Results and Discussion

The single layer graphene on mica was prepared with the mechanical exfoliation method in air and at room temperature. The water molecules are easily confined between graphene and mica in air due to the high hydrophilicity of mica surface. This intercalated water adlayer was confirmed by FFM with high spatial resolution at ambient conditions (relative humidity 45 ~ 50 %, temperature 22 ~ 24 ℃), as shown in Figure 1. The two-dimensional (2D) first and second ice-like water adlayer are clearly visible at the upper right half of topography in Figure 1a. The topography and friction images show the regions of mica, single-graphene (SLG) + zero ice-like water layer (0W), SLG + first ice-like water layer (1W), and SLG + second ice-like water layer (2W) in Figure 1a and 1b. (*i.e.*, the single graphene layer on the first ice-like water layer on mica is denoted by SLG+1W on mica to simplify denotation as discussed below.) The bright contrast means the higher friction in Figure 1b. The friction images clearly show the friction increase by the intercalation of ice-like water layer between graphene and mica. The friction depending on the thickness of the intercalated water is precisely observed as shown in Figure 1b. The higher friction on SLG+2W is revealed as compared with that on SLG+1W.

In addition, more results exhibiting enhanced friction of SLG and bilayer graphene (BLG) by water intercalation are shown in Figure 2. The SLG and BLG on mica samples with 1W were prepared at ambient conditions. The shape of the confined water layer is clearly distinguishable in the topography in Figure 2a. The bright portion of the longitudinal stripe is caused by MLG. The friction image was simultaneously acquired with the topographical image, clearly showing a higher friction domain in the center of the graphene layer caused by water intercalated between the graphene and mica, as shown in Figure 2b. Figure 2c and 2d shows magnified topography and friction images from the blue box in Figure 2b. Areas *a*, *b*, and *c* in Figure 2c are bare mica, SLG+0W on mica, and SLG+1W on mica, respectively. The shape of the 1W domain in the topography image is equal to the high-friction domain on the graphene in Figure 2d. The height of the SLG on bare mica is ~0.6 nm, which value is comprehensible due to the sensitivity of AFM measurements, and that of 1W appears to be ~0.37 nm in Figure 2e.

We investigated the dependence of friction on graphene thickness and on the thickness of the intercalated water. Areas *d*, *e*, *f*, and *g* in Figure 2c are BLG+1W on mica, BLG+0W on mica, SLG+0W on mica, and bare mica, respectively. The BLG is ~0.94 nm in height and appears as an inverted triangular shape in the upper left corner of Figure 2c. The increased friction induced by water intercalation in BLG is less visible compared with the friction enhancement in SLG, but is still higher than on the BLG+0W on mica, as shown in Figure 2d and 2f. On the other hand, the friction on BLG on mica and SLG on mica without water is the same, as was also seen in previous report[18]. In here, the friction images from several numbers of graphene layers with intercalated water were also acquired. The effect of water on friction decreases as the number of graphene layers increases. Figure 2g show a schematic representation of the variation in friction over graphene layers with and without intercalated water using a tilted AFM tip; the labels *a–g* match those along the lines in Figure 2c.

The high resolution KPFM was performed on water-intercalated graphene on mica at constant RH and room temperature (~47% and 23 °C), as shown in Figure 3. The intercalated water layer between graphene and mica was clearly detected at the upper left half of topography in Figure 3a. In addition, the small second and third ice-like water adlayer also are observed on the first ice-like water adlayer. The measured height of single layer graphene on the fresh bare mica surface is 0.65 nm. The first, second, and third ice-like water adlayer show the height of ~0.37 nm. This value is well matched with the interlayer distance of a single puckered bilayer in the bulk ice structure[10]. The areas by labelled I, II, III, IV, and V are SLG+1W, SLG+0W, SLG+3D liquid-like water droplet, and multi-graphene (MLG)+0W on mica, and bare mica in Figure 3a, respectively. The surface potential image clearly shows the different contrast, depending on the sublayer composition, as shown in Figure 3b. The blue to red color means the low to high contact potential difference (CPD) in Figure 3b. Figure 3c shows that the cross-profiles along the yellow solid lines in topography and surface potential images. The areas of I and IV show the higher CPD of ~40 mV and ~90 mV than that of II area. If we assume that the IV area have the same graphite work function (4.6 eV) [28-30], I and II have the work function of 4.65 eV and 4.69 eV, respectively. The III area occupied water droplet as ~3 nm in height shows the even lower work function than at I. These phenomena are well matched with a previous work, which shows that they were caused by reducing the charge transfer between graphene and mica by intercalated water molecules, while the mica induce the *p*-type doping effects in graphene[28]. In addition, the Raman spectra at water intercalated graphene on mica was also obtained before and after vacuum annealing (400 ℃ for 2h under 3.5×10^{-3} Torr) for more evidence of water existence and doping effects between graphene and mica, as shown in Figure 4. Figure 4a shows the three major peaks such as G, 2D, and OH mode from mica between 1200 ~ 4000 cm^{-1} Raman shift in both cases. The shaper and higher 2D intensity than that of G (*i.e.*, the ratio of I_{2D}/I_G is over 2) and absent D peak (~1350 cm^{-1}) mean that the mechanical exfoliated graphene on mica is monolayer pristine graphene and has less defect density[31-34]. However, the ratio of I_{2D}/I_G is reduced after vacuum annealing due to the higher substrate effects in Figure 4a[35-38]. Figure 4b and 4c show that the G and 2D band frequencies have the downshifts before vacuum annealing because the interfacial charge transfer (*p*-doping effect from mica substrates) is effectively blocked by water adlayer between graphene and mica. The OH mode frequency is dominated by mica substrates[10].

Figure 5 shows atomic stick–slip behavior in friction for SLG on mica with 0W, 1W, and 2W intercalated layers. The friction loops with a scan distance of 4 nm, which are composed of trace and retrace signals, show the atomic stick–slip behavior at SLG+0W, SLG+1W, and SLG+2W in Figure 5a–c. The slope of the friction loops (α, marked by the dotted black line), which depends on the magnitude of the slip motion in a period, represents the so-called “strengthening” effect[18]. In Figure 5a–c, the measured friction loop of SLG on a water layer is slightly more tilted than that of SLG+0W because the hydrophobic pristine graphene has a weak interaction with the water layer, while the water molecules are tightly bound to the surface of hydrophilic mica via hydrogen bonding. However, similar slopes are seen for SLG+1W and SLG+2W in Figure 5b and 5c. This indicates that the puckering effect can only partly explain the increased friction by intercalated water, but not explain the enhanced friction by the increased number of intercalated water layers. The measured α for SLG+0W, SLG+1W, and SLG+2W are shown in Figure 5d. The total lateral stiffness (k_{total}) can also be compared by using the slope of the atomic stick–slip curves. Figure 5a–c shows the slopes of the atomic stick–slip curves for SLG+0W, SLG+1W, and SLG+2W, which are marked by the dotted red lines. The measured k_{total} of SLG+0W, SLG+1W, and SLG+2W have similar values as shown in Figure 5d.

Figure 6 shows topographic and friction images of the graphene on mica after intercalation of D_2O between the graphene on mica, which was accomplished by exposure of the sample to high D_2O humidity (99%) for 12 h. The first topography and friction images were acquired after graphene deposition in air (45~50% RH). Figure 6a and 6b shows a patch of 1W in the central region of a SLG flake exhibiting a 3-fold increase in friction over the 1W patch, as discussed in the previous section[39]. After D_2O intercalation, topographic and friction images (Figure 6c and 6d) were acquired in the same sample region at laboratory conditions (RT, 45% RH). In the topography image, the dashed line marks the boundary of the 1W patch and shows the expansion of the intercalated water region, which is now a mixture of D_2O + H_2O. We clearly observe a substantially smaller increase (by a factor of 1.5) in the friction force over the D_2O + H_2O region (Figure 6d) compared with that of pure H_2O. This is shown in the plot of normalized friction values in Figure 6e.

The presence of D_2O between graphene and mica is confirmed by Fourier transform infrared (FTIR) spectra, which shows the peaks from O–D stretch bonds, as shown in Figure 6f [40]. Bare mica surfaces (i.e. with no graphene deposited) after the same exposure to D_2O (99% RH for 20 h), but analyzed in 45% RH laboratory air, show no O–D stretch bond peaks. This indicates that the peaks in Figure 6f are produced only by the intercalated water. As explained above, intercalated water diffuses very slowly, but molecular exchange with the ambient vapor is fast in the open mica areas. We could not quantitatively determine the D_2O:H_2O density ratio because the H-stretch region of the FTIR is dominated by H vibrations from OH and H_2O in the uncovered mica areas and in the bulk mica.

To understand the increase of friction caused by intercalated water, we examined phonon DOS of SLG+0W, SLG+1W, and SLG+2W on mica, obtained from first-principles density functional theory (DFT) calculations. Figure 7a-c reveal the side views of relaxed atomic structures of SLG+0W, SLG+1W, and SLG+2W on mica, respectively. Figure 7d shows projected phonon DOS of graphene and water for SLG+0W, SLG+1W, and SLG+2W on mica, respectively. The dash and solid line in Figure 7d represents in-plane and out-of-plane phonon modes, respectively. Phonon DOS of graphene with water layers reveal new out-of-plane phonon modes at low frequency regime (< 5 THz) due to interaction between graphene and water layer, compared to graphene without water layers. Contrary to the out-of-plane phonon modes, in-plane phonon modes of graphene are almost not changed. It means that phonon modes of water layers are strongly interacted with out-of-plane or flexural phonon of graphene. Note that we only focused on phonon frequency between 0 and 16 THz because it is phonon frequency range of Si, which is tip material. To find what phonon modes of water layer are interacted with flexural phonon of graphene, we examined the phonon DOS of water layer, as shown in Fig. 7d (bottom). For SLG+1W on mica, while in-plane phonon modes of water layer is slightly interacted with flexural phonon of graphene at 1 THz, out-of-plane phonon modes of water layer is strongly interacted with flexural phonon of graphene by generating the new flexural phonon modes near 3.5 THz. Thus, frictional energy of SLG+1W could be mostly dissipated via flexural phonon interacted with out-of-plane phonon modes of water layer. The reason why friction of SLG+2W on mica is higher than that of SLG+1W on mica is also associated with flexural phonon interacted with out-of-plane phonon modes of water layer. Figure 7d (bottom) shows that out-of-plane phonon modes of water layers for SLG+2W on mica are generated near 2.5 THz because of water-water interaction, compared to those for SLG+1W on mica. It indicates that SLG+2W on mica has more phonon channel to dissipate the frictional energy from graphene surface to mica substrate.

The increased out-of-plane phonon modes of graphene and water provide new channels for excitation that can absorb the kinetic energy of moving bodies. Flexural deformation of graphene, which manifests in ripples (puckering deformation), has been observed before and shown to increase friction by a factor of 2[18]. However, the increase observed with intercalated water is even larger, indicating additional effects from the water. The additional effects include the presence of low-frequency phonon modes of water and the contribution of high-frequency modes of water, such as stretch and bending vibration modes involving H or D atoms, as supported by the multilayer effect of water and the large isotope effect observed here, as shown in Figure 8. D_2O intercalation leads the decrease of friction at H_2O intercalated graphene on mica due to the low vibrational frequency of D_2O adsorbate, which means the low rate of frictional energy dissipation at the interface as the difference of phonon contribution. The phonon DOS of graphene and mica for SLG+1W (H_2O) and (D_2O) are not changed at the whole frequency regime as shown in Figure 8b, while the phonon DOS of D_2O show the lower vibrational frequency than those of H_2O due to the higher mass of D_2O molecules in Figure 8. For this isotope effect, a similar result was observed by Cannara *et al.* in their study of the friction properties of H- and D-terminated Si and C films[3]. These authors conclude that the faster collision rate of H atoms vs D atoms with the substrate increases the efficiency of energy transfer, a conclusion that is also supported by the present results.

4. Conclusions

In conclusion, we have found the phononic friction phenomena on H_2O and D_2O intercalated graphene on mica substrates as an isotope and thickness-dependent effects using friction force microscopy. The confined water layer composed of H_2O molecules between graphene and mica induce the enhancement of friction on graphene, and it depends on thickness of intercalated ice-like water layer and covered graphene sheet. On the other hand, D_2O intercalation leads the decrease of friction at H_2O intercalated graphene on mica due to the low vibrational frequency of D_2O adsorbate, representing the low rate of frictional kinetic energy dissipation at the interface as the difference of phonon contribution. Using the first-principles DFT calculations, the quantitative approach of friction change along the vibrational frequencies of water molecule adsorbates was performed on the interface between graphene and mica. These results suggest that the system of graphene/water/mica can be readily treated to understand the phonon contribution on frictional energy dissipation.

References

[1] Persson, B.N.: Sliding friction: physical principles and applications. Springer Science & Business Media, (2000)

[2] Park, J.Y., Salmeron, M.: Fundamental aspects of energy dissipation in friction. Chem. Rev. **114**(1), 677-711 (2014)

[3] Cannara, R.J., Brukman, M.J., Cimatu, K., Sumant, A.V., Baldelli, S., Carpick, R.W.: Nanoscale friction varied by isotopic shifting of surface vibrational frequencies. Science **318**(5851), 780-783 (2007)

[4] Park, J.Y., Ogletree, D., Thiel, P., Salmeron, M.: Electronic control of friction in silicon pn junctions. Science **313**(5784), 186-186 (2006)

[5] Kisiel, M., Gnecco, E., Gysin, U., Marot, L., Rast, S., Meyer, E.: Suppression of electronic friction on Nb films in the superconducting state. Nat. Mater. **10**(2), 119-122 (2011)

[6] Kietzig, A.-M., Hatzikiriakos, S.G., Englezos, P.: Physics of ice friction. J. Appl. Phys. **107**(8), 081101 (2010)

[7] Bluhm, H., Inoue, T., Salmeron, M.: Friction of ice measured using lateral force microscopy. Phys. Rev. B **61**, 7760 (2000)

[8] Geim, A.K., Novoselov, K.S.: The rise of graphene. Nat. Mater. **6**, 183-191 (2007)

[9] Zhang, Y., Tan, Y.-W., Stormer, H.L., Kim, P.: Experimental observation of the quantum Hall effect and Berry's phase in graphene. Nature **438**, 201-204 (2005)

[10] Xu, K., Cao, P., Heath, J.R.: Graphene visualizes the first water adlayers on mica at ambient conditions. Science **329**(5996), 1188-1191 (2010)

[11] Severin, N., Lange, P., Sokolov, I.M., Rabe, J.P.: Reversible dewetting of a molecularly thin fluid water film in a soft graphene–mica slit pore. Nano Lett. **12**(2), 774-779 (2012)

[12] Li, Q., Song, J., Besenbacher, F., Dong, M.: Two-dimensional material confined water. Acc. Chem. Res. **48**(1), 119-127 (2015)

[13] Hu, J., Xiao, X., Ogletree, D., Salmeron, M.: Imaging the condensation and evaporation of molecularly thin films of water with nanometer resolution. Science **268**(5208), 267 (1995)

[14] Kim, J.-S., Choi, J.S., Lee, M.J., Park, B.H., Bukhvalov, D., Son, Y.-W., et al.: Between scylla and charybdis: hydrophobic graphene-guided water diffusion on hydrophilic substrates. Sci. Rep. **3** (2013)

[15] Song, J., Li, Q., Wang, X., Li, J., Zhang, S., Kjems, J., et al.: Evidence of Stranski–Krastanov growth at the initial stage of atmospheric water condensation. Nat. Commun. **5** (2014)

[16] Severin, N., Gienger, J., Scenev, V., Lange, P., Sokolov, I.M., Rabe, J.P.: Nanophase separation in monomolecularly thin water–ethanol films controlled by graphene. Nano Lett. **15**(2), 1171-1176 (2015)

[17] Cheng, M., Wang, D., Sun, Z., Zhao, J., Yang, R., Wang, G., et al.: A route toward digital manipulation of water nanodroplets on surfaces. ACS Nano **8**(4), 3955-3960 (2014)

[18] Lee, C., Li, Q., Kalb, W., Liu, X.-Z., Berger, H., Carpick, R.W., et al.: Frictional characteristics of atomically thin sheets. Science **328**(5974), 76-80 (2010)

[19] Choi, J.S., Kim, J.-S., Byun, I.-S., Lee, D.H., Lee, M.J., Park, B.H., et al.: Friction anisotropy–driven domain imaging on exfoliated monolayer graphene. Science **333**(6042), 607-610 (2011)

[20] Filleter, T., McChesney, J.L., Bostwick, A., Rotenberg, E., Emtsev, K.V., Seyller, T., et al.: Friction and dissipation in epitaxial graphene films. Phys. Rev. Lett. **102**(8), 086102 (2009)

[21] Kwon, S., Ko, J.-H., Jeon, K.-J., Kim, Y.-H., Park, J.Y.: Enhanced nanoscale friction on fluorinated graphene. Nano Lett. **12**(12), 6043-6048 (2012)

[22] Li, Q., Liu, X.-Z., Kim, S.-P., Shenoy, V.B., Sheehan, P.E., Robinson, J.T., et al.: Fluorination of graphene enhances friction due to increased corrugation. Nano Lett. **14**(9), 5212-5217 (2014)

[23] Ko, J.-H., Kwon, S., Byun, I.-S., Choi, J.S., Park, B.H., Kim, Y.-H., et al.: Nanotribological properties of fluorinated, hydrogenated, and oxidized graphenes. Tribol. Lett. **50**(2), 137-144 (2013)

[24] Dong, Y., Wu, X., Martini, A.: Atomic roughness enhanced friction on hydrogenated graphene. Nanotechnology **24**, 375701 (2013)

[25] Allen, M.J., Tung, V.C., Kaner, R.B.: Honeycomb carbon: a review of graphene. Chem. Rev. **110**(1), 132-145 (2009)

[26] Ogletree, D., Carpick, R.W., Salmeron, M.: Calibration of frictional forces in atomic force microscopy. Rev. Sci. Instrum. **67**(9), 3298-3306 (1996)

[27] Varenberg, M., Etsion, I., Halperin, G.: An improved wedge calibration method for lateral force in atomic force microscopy. Rev. Sci. Instrum. **74**(7), 3362-3367 (2003)

[28] Shim, J., Lui, C.H., Ko, T.Y., Yu, Y.-J., Kim, P., Heinz, T.F., et al.: Water-gated charge doping of graphene induced by mica substrates. Nano Lett. **12**(2), 648-654 (2012)

[29] Takahashi, T., Tokailin, H., Sagawa, T.: Angle-resolved ultraviolet photoelectron spectroscopy of the unoccupied band structure of graphite. Phys. Rev. B **32**, 8317-8324 (1985)

[30] Yu, Y.-J., Zhao, Y., Ryu, S., Brus, L.E., Kim, K.S., Kim, P.: Tuning the graphene work function by electric field effect. Nano Lett. **9**(10) 3430-3434 (2009)

[31] Ferrari, A., Meyer, J., Scardaci, V., Casiraghi, C., Lazzeri, M., Mauri, F., et al.: Raman spectrum of graphene and graphene layers. Phys. Rev. Lett. **97**(18), 187401 (2006)

[32] Dresselhaus, M.S., Jorio, A., Hofmann, M., Dresselhaus, G., Saito, R.: Perspectives on carbon nanotubes and graphene Raman spectroscopy. Nano Lett. **10**(3), 751-758 (2010)

[33] Ferrari, A.C.: Raman spectroscopy of graphene and graphite: disorder, electron–phonon coupling, doping and nonadiabatic effects. Solid State Commun. **143**(1-2), 47-57 (2007)

[34] Malard, L., Pimenta, M., Dresselhaus, G., Dresselhaus, M.: Raman spectroscopy in graphene. Physics Reports **473**(5-6), 51-87 (2009)
[35] Lee, D., Ahn, G., Ryu, S.: Two-dimensional water diffusion at a graphene–silica interface. J. Am. Chem. Soc. **136**(18), 6634-6642 (2014)
[36] Berciaud, S., Ryu, S., Brus, L.E., Heinz, T.F.: Probing the intrinsic properties of exfoliated graphene: Raman spectroscopy of free-standing monolayers. Nano Lett. **9**(1), 346-352 (2008)
[37] Campos-Delgado, J., Kim, Y., Hayashi, T., Morelos-Gómez, A., Hofmann, M., Muramatsu, H., et al.: Thermal stability studies of CVD-grown graphene nanoribbons: Defect annealing and loop formation. Chem. Phys. Lett. **469**(1-3), 177-182 (2009)
[38] Ni, Z., Wang, Y., Yu, T., Shen, Z.: Raman spectroscopy and imaging of graphene. Nano Res. **1**, 273-291 (2008)
[39] Lee, H., Ko, J.-H., Choi, J.S., Hwang, J.H., Kim, Y.-H., Salmeron, M., et al. Enhancement of friction by water intercalated between graphene and mica. J. Phys. Chem. Lett. **8**, 3482-3487 (2017)
[40] He, K.T., Wood, J.D., Doidge, G.P., Pop, E., Lyding, J.W.: Scanning tunneling microscopy study and nanomanipulation of graphene-coated water on mica. Nano Lett. **12**(6), 2665-2672 (2012)
[41] Perdew, J. P., Burke, K., Ernzerhof, M.: Generalized Gradient Approximation Made Simple. Phys. Rev. Lett. **77**(18), 3865−3868 (1996)
[42] Kresse, G., Joubert, D.: From Ultrasoft Pseudopotentials to the Projector Augmented-Wave Method. Phys. Rev. B **59**(3), 1758−1775 (1999)
[43] Kresse, G., Furthmüller, J.: Efficient Iterative Schemes for Ab Initio Total-Energy Calculations Using a Plane-Wave Basis Set. Phys. Rev. B **54**(16), 11169−11186 (1996)
[44] Blöchl, P. E.: Projector Augmented-Wave Method. Phys. Rev. B **50**(), 17953 (1994)
[45] Grimme, S.: Semiempirical GGA-Type Density Functional Constructed with a Long-Range Dispersion Correction. J. Comput. Chem. **27**(15), 1787−1799 (2006)
[46] Parlinski, K., Li, Z., Kawazoe, Y.: First-Principles Determination of the Soft Mode in Cubic ZrO2. Phys. Rev. Lett. **78**(21), 4063 (1997)
[47] Togo, A., Oba, F., Tanaka, I.: First-Principles Calculations of the Ferroelastic Transition between Rutile-Type and $CaCl_2$-Type SiO_2 at High Pressures. Phys. Rev. B **78**(13), 134106 (2008)

Acknowledgements

This work was supported by the Institute for Basic Science [IBS-R004-A2-2017-a00]. M.S. was supported by the Office of Basic Energy Sciences, Division of Materials Sciences and Engineering, of the U.S. Department of Energy, under Contract No. DE-AC02-05CH11231, (FWP KC3101). J.-H.K. and Y.-H.K. were supported by the NRF (2015R1A2A2A05027766), SRC (2016R1A5A1008184), and Global Frontier R&D (2011-0031566) programs of Korea.

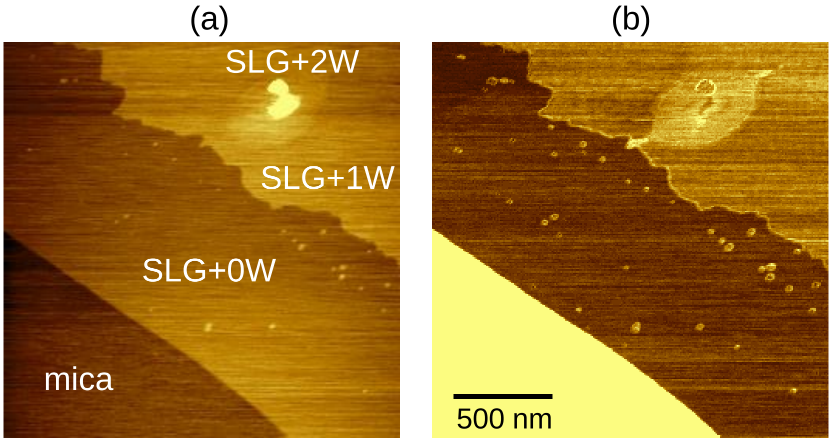

Fig. 1. **a** 2.0 μm × 2.0 μm topography and **b** friction images of water-intercalated graphene on mica.

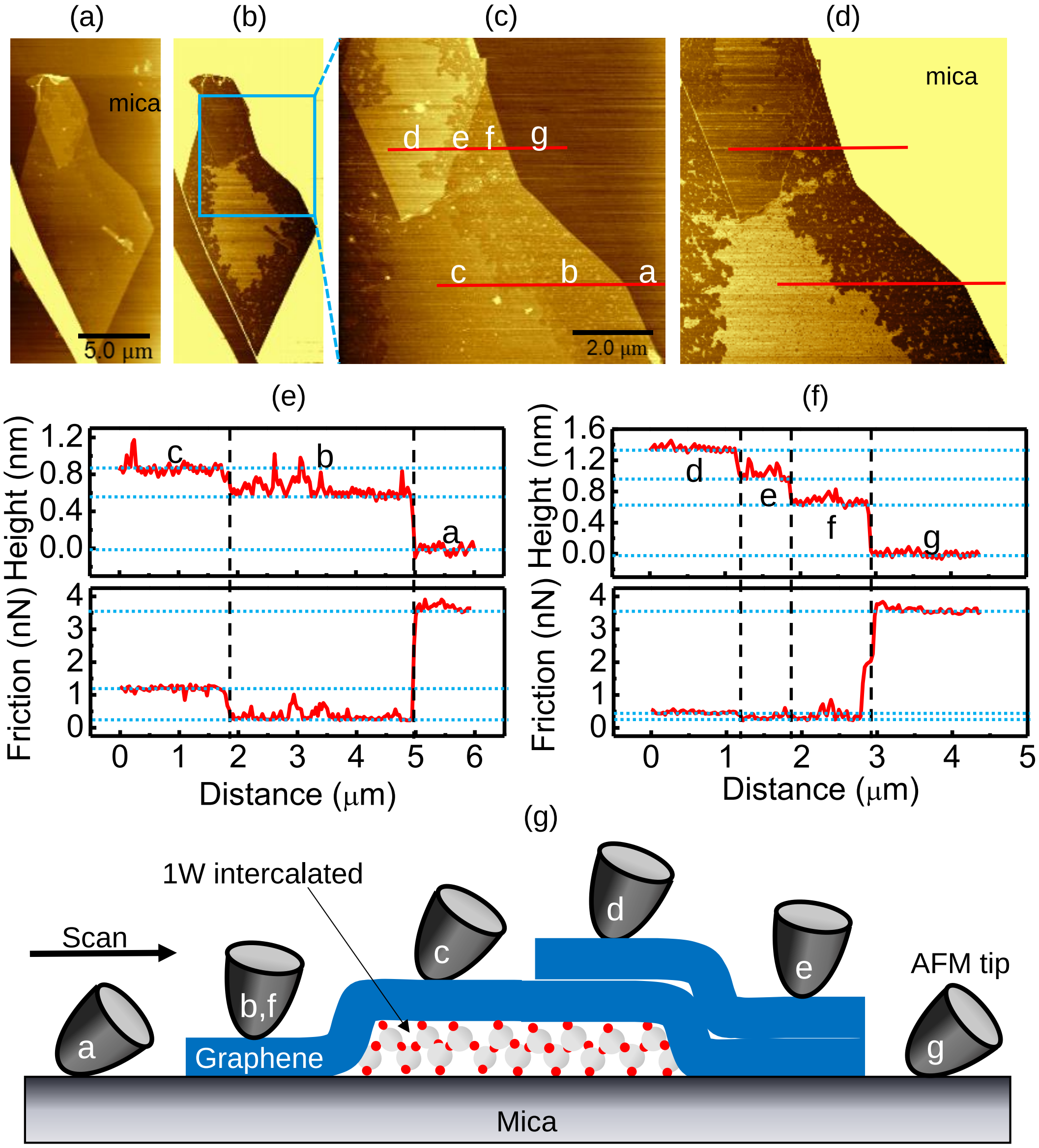

Fig. 2. **a** Topography and **b** friction images (11 μm × 24 μm) of water-intercalated graphene on mica after mechanical cleavage in air. **c** Magnified topography and **d** friction images (7 μm × 7 μm) from the blue box in **b** measured simultaneously at an applied force of 9.6 nN where the labels represent *a* bare mica, *b* SLG, *c* SLG+1W, *d* BLG+1W, *e* BLG, *f* SLG, and *g* bare mica. (**e**, **f**) Line profiles of the height and friction along the red lines in **c** and **d** for *a*–*c* and *d*–*g*, respectively. (**g**) Schematic diagram showing the variable friction behavior using a tilted AFM tip, depending on the sublayer composition. Labels *a*–*g* in the tip match areas *a*–*g* in **c**.

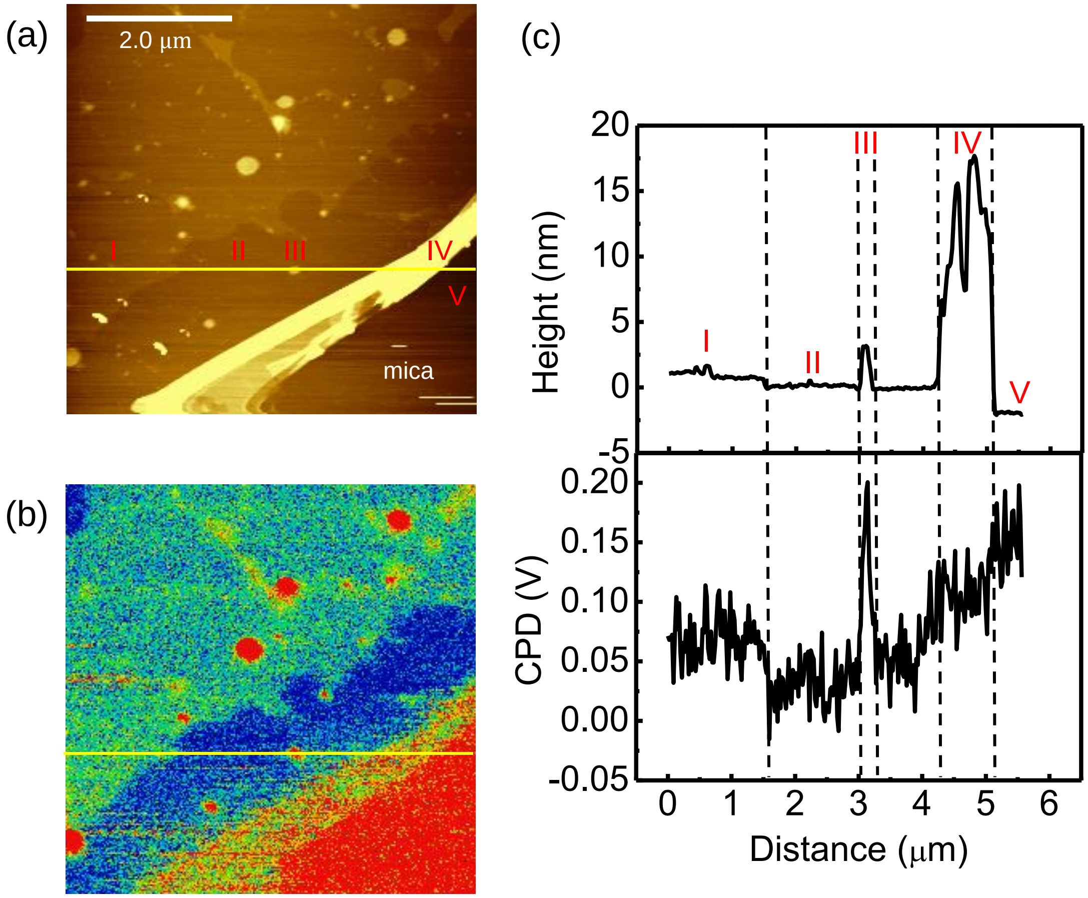

Fig. 3. **a** 5.5 μm × 5.5 μm topography and **b** surface potential images of the water intercalated graphene on mica using KPFM measurement at ambient conditions. **c** Line profiles of the height and CPD along the yellow solid line in **a** and **b**. The labels I, II, III, IV, and V represent the SLG+1W, SLG+0W, SLG+3D liquid-like water droplet, MLG+0W on mica, and bare mica, respectively.

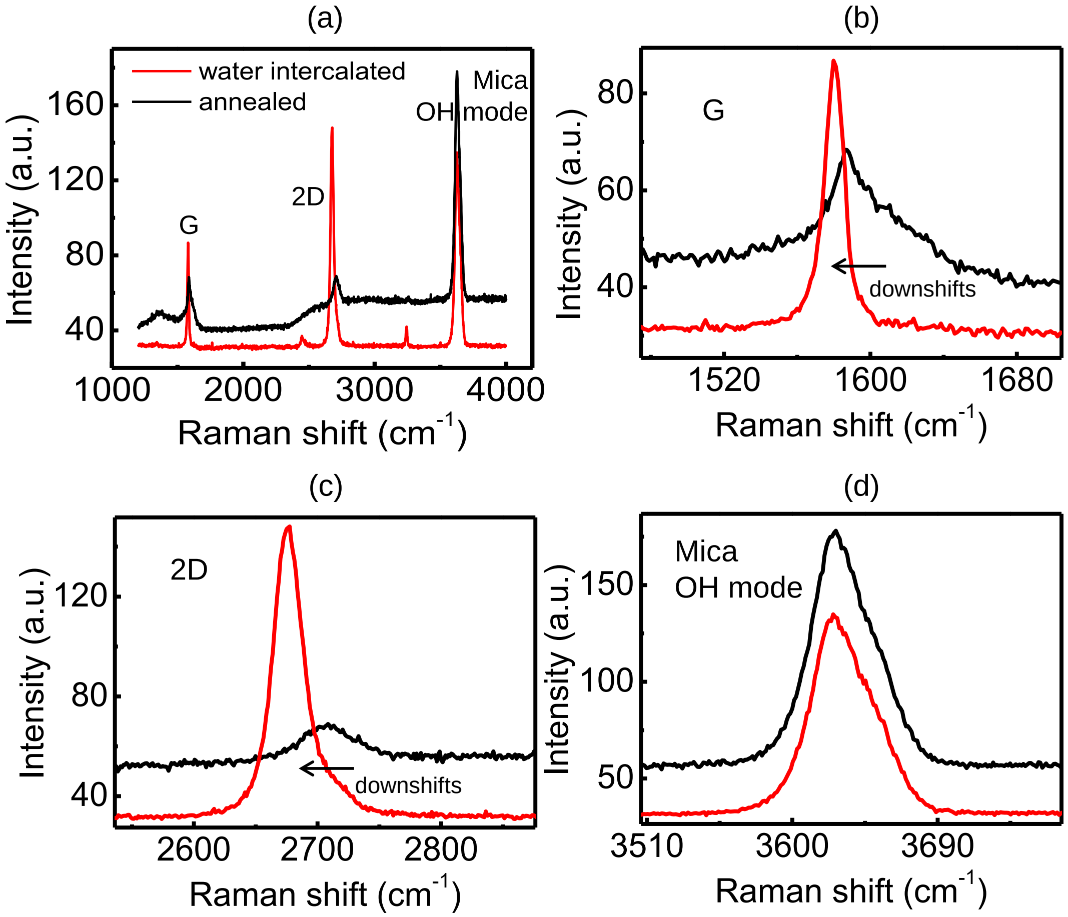

Fig. 4. a Raman spectra of water intercalated graphene on mica before (water intercalated) and after (annealed) vacuum annealing (400 ℃ for 2h under 3.5×10^{-3} Torr). **b** G, **c** 2D band frequencies, and **d** mica OH mode.

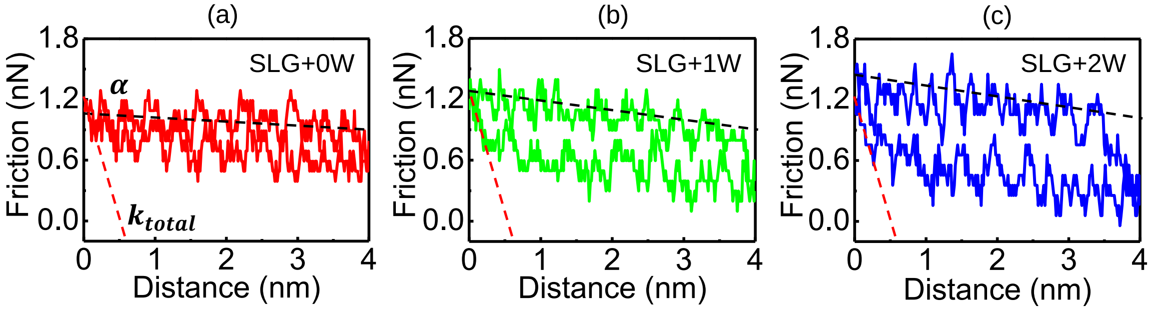

(d)

	SLG+0W	SLG+1W	SLG+2W
α (mN/m)	56.3±10.4	95.2±13.9	94.2±7.1
k_{total} (N/m)	2.3±0.1	2.0±0.3	2.1±0.2

Fig. 5. (**a**–**c**) Friction loops with a 4 nm scan width of SLG+0W, SLG+1W, and SLG+2W. **d** The measured slopes of the friction loops (α) and atomic stick–slip curves (k_{total}).

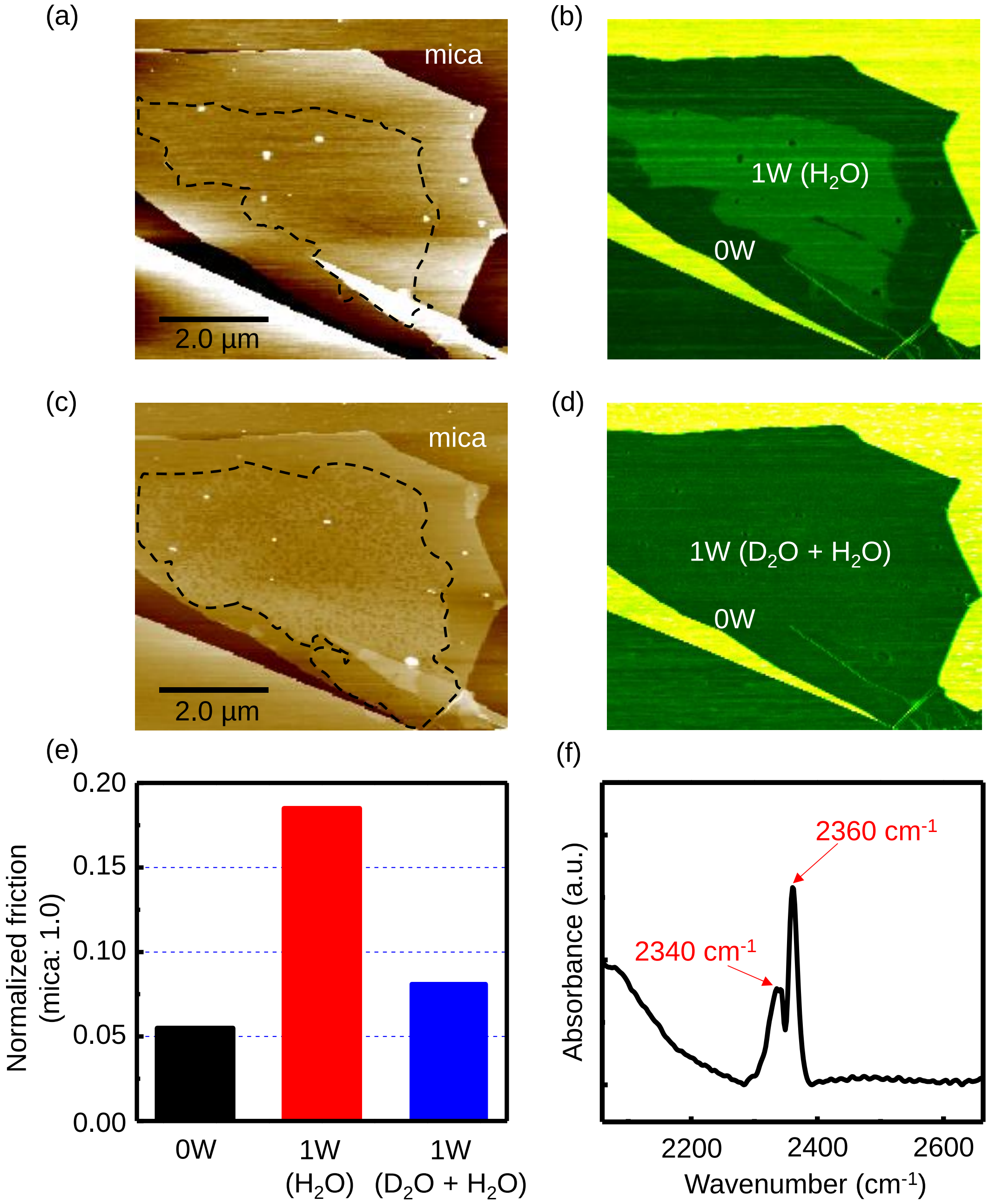

Fig. 6. **a** Topography and **b** friction images (6.2 μm × 6.8 μm) of graphene on mica with an applied force of 9.6 nN. A large patch of intercalated H_2O-water is present in the center. **c** Topography and **d** friction images (6.2 μm × 6.8 μm) of the same area after exchanging the H_2O with D_2O following a 12 h exposure at 99% RH of D_2O vapor. The images were acquired at ambient laboratory air (45% RH). Only the intercalated water

remained deuterated, while the water layer in the exposed mica regions reverted to back H_2O following rapid equilibration with the ambient humidity. **e** Plot showing the increased friction on graphene on mica with intercalated H_2O and H_2O + D_2O. The friction values were normalized with that on mica (=1). **f** FTIR spectra showing the O–D stretch modes of D_2O in the intercalated water.

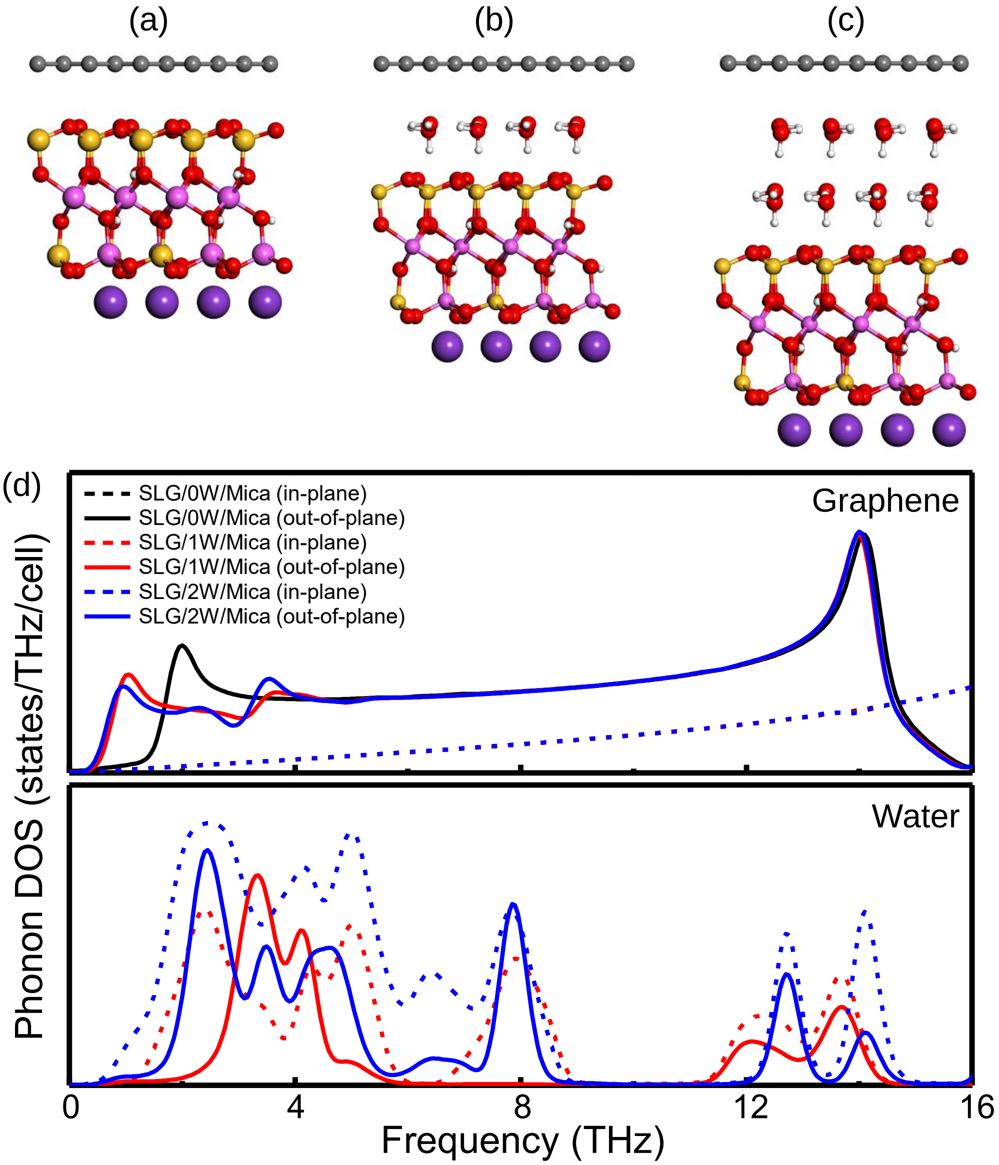

Fig. 7. Optimized atomic structures of **a** SLG/0W/Mica, **b** SLG/1W/Mica, and **c** SLG/2W/Mica (gray, C; red, O; orange, Si; purple, Al; and white, H). **d** Projected phonon density of states of graphene (top) and water (bottom) for SLG/0W/Mica (black), SLG/1W/Mica (red), and SLG/2W/Mica (blue), respectively. Dash and solid lines represent the in-plane and out-of-plane phonon modes, respectively.

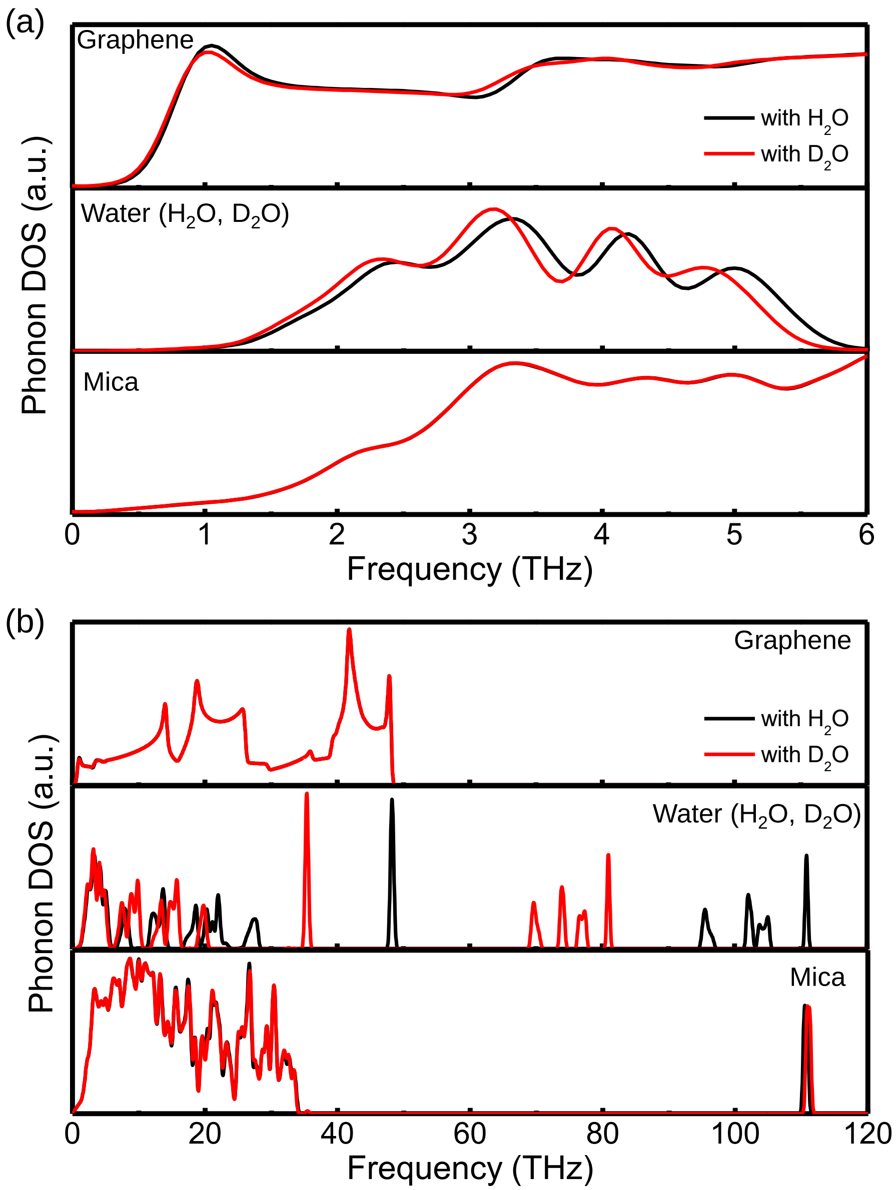

Fig. 8. a and **b** Projected phonon density of states of graphene (top), water layers (middle), and mica (bottom) for SLG+1W (H_2O) (black), and SLG+1W (D_2O) (red) at low frequency regime (< 6 THz) and full frequency regime, respectively.